International Journal of Solids and Structures 49 (2012) 3170–3184

Contents lists available at SciVerse ScienceDirect

International Journal of Solids and Structures

journal homepage: www.elsevier.com/locate/ijsolstr

Calculation of near-tip non-singular stresses for pressurized cracks

J.H. Chang *, T.Y. Guo

Department of Civil Engineering, National Central University, Taoyuan County, Jhongli 32001, Taiwan

ARTICLE INFO

Article history:
Received 10 January 2012
Received in revised form 25 June 2012
Available online 20 July 2012

Keywords:
Pressurized crack
Asymptotic non-singular stresses
T-stress
Stress intensity factors
Auxiliary stress field
De-singularized loading system

ABSTRACT

When the crack surfaces are traction-free, there is only one constant term T in the near-tip stress field, which contributes uniformly to the stress component acting in the direction parallel to the crack flank. As to pressurized cracks, the non-singular part of the asymptotic stresses appears to be more complicated and is no longer characterized only by the constant T. In this work, an effective numerical approach is developed for calculation of the non-singular parts of the asymptotic near-tip stresses under the action of nonuniform crack surface pressures. With this approach, the near-tip non-singular stress field can be accurately evaluated by direct use of regular numerical methods such as finite elements.

1. Introduction

The asymptotic stress field in the immediate neighborhood of a crack tip consists of the singular and the non-singular (i.e., finite-valued) parts. In many engineering applications, nonuniform pressures along the crack surfaces—which may be due to pressurized fluids, contact pressure, etc.—are of special interest. In such cases, the near-tip stress depends significantly on the pressurized condition. On one hand, the singular stress field is characterized by a pair of stress intensity factors (SIFs), which can be effectively determined by using a number of well-developed approaches (as reviewed by, e.g., Chang and Wu (2007)). On the other hand, direct evaluation of the non-singular part of stresses appears to be difficult due to the singular-dominant feature around the crack tip. More investigations on proper approaches for calculation of the asymptotic non-singular stresses are therefore in need.

When the crack surfaces are traction-free, the asymptotic non-singular stress field is characterized by one constant term, i.e., the T-stress T. The T-stress acts uniformly in the direction parallel to the crack flank and is crucial to engineering fracture analysis. A variety of approaches have thus been performed for determination of the T-stress. For problems under specific geometric and loading conditions, the contribution of T-stress can be determined by using analytical approaches such as singular integral equations (e.g., Wang, 2003; Broberg, 2005), weight functions (Sham, 1991; Fett and Rizzi, 2005). and specific closed form equations (e.g., Chen et al., 2010), etc. Also, the T-stress can be numerically evaluated by using the near-tip displacement and/or stress fields extracted directly from finite element solutions (e.g., Eischen, 1987; Wang and Parks, 1992, etc.). Alternatively, the T-stress can be evaluated by using various types of interaction contour integrals (e.g., Nakamura and Parks, 1991; Moon and Earmme, 1998; Sladek et al., 1997), In addition, numerical approaches in conjunction with finite element method have been presented for calculation of T (e.g., Jogdand and Murthy, 2010).

For the condition of pressurized cracks, the non-singular part of the asymptotic stresses appears to be more complicated and is no longer characterized only by the constant T. As a matter of fact, when the crack surfaces are subjected to nonuniformly-distributed pressures, the corresponding asymptotic non-singular stresses are also anticipated to be nonunifiormly distributed in the near-tip area due to the influence of the higher order terms. Nevertheless, to the authors' best knowledge, while study on evaluation of the T-stress for pressurized cracks has been preformed (e.g.,, Wang, 2002), very few discussions in the literature have been devoted to calculation of these higher order terms and more relevant studies are still in need.

In this paper, an effective numerical procedure is developed for calculating the non-singular part of the asymptotic near-tip stresses due to the action of nonuniform pressures along the crack surfaces. Through proper definition of auxiliary stress fields, the non-singular stress field can be directly extracted from 'regular' finite element solutions, with no need of special treatment. Since the auxiliary stress fields can be easily constructed by using finite elements. this presented approach thus appears to be applicable for problems with arbitrary spatial distribution of crack surface pressures. No particular singular elements are used in the study.

* Corresponding author. Tel.: +886 3 4227151; fax: +886 3 4252960.
E-mail address: t320001@cc.ncu.edu.tw (J.H. Chang).

0020-7683/$ - see front matter © 2012 Elsevier Ltd. All rights reserved.
http://dx.doi.org/10.1016/j.ijsolstr.2012.06.015

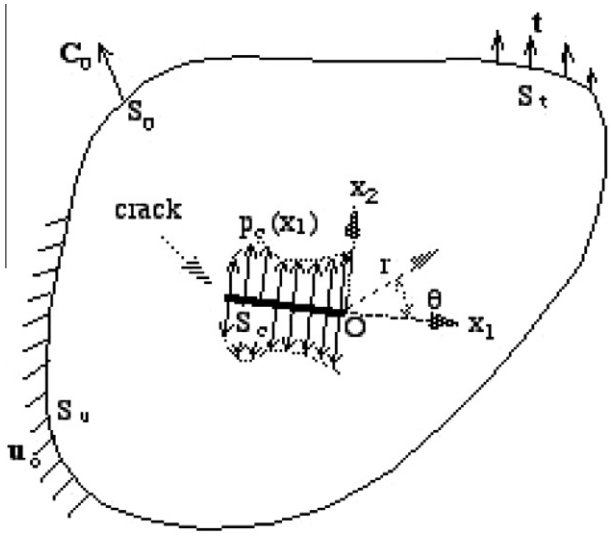

Fig. 1. A pressurized crack in a 2D elastic body with a local coordinate system.

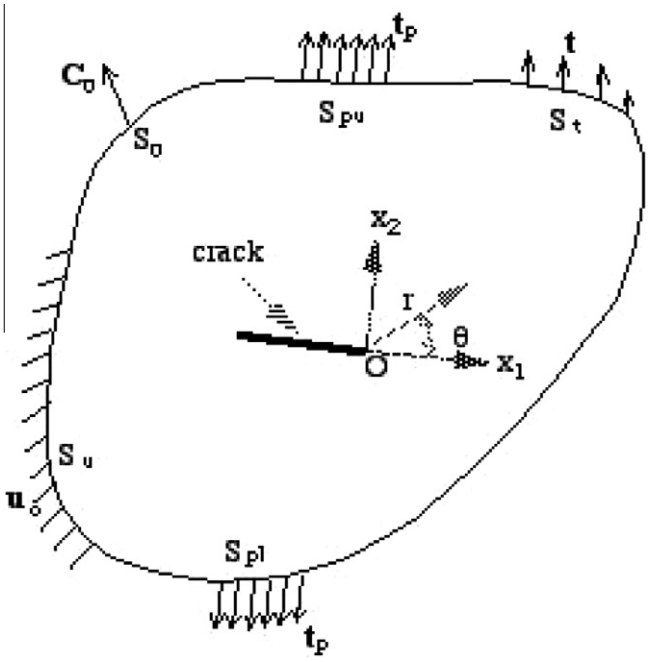

Fig. 2. The crack surface pressures are replaced by $\mathbf{t}_p$ on S_{pu} and S_{pl}

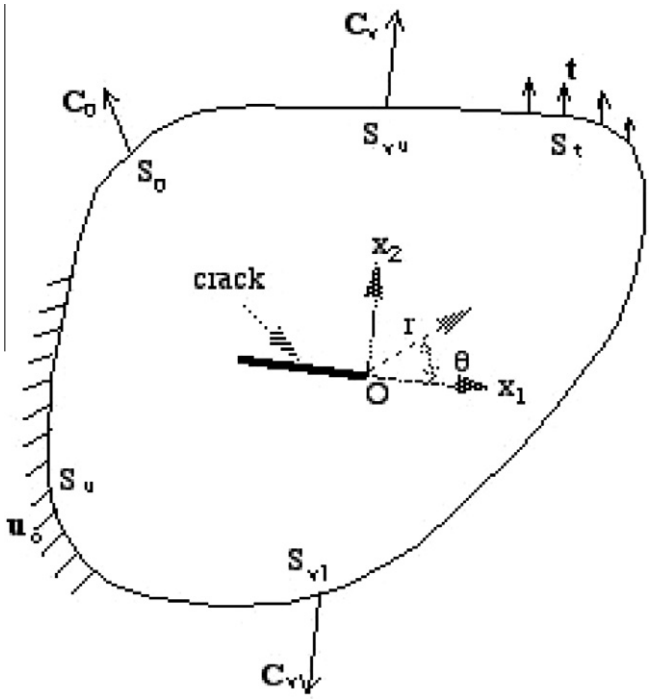

Fig. 3. The crack surface pressures are replaced by $\mathbf{C}_V$ at points S_{Vu} and S_{Vl}.

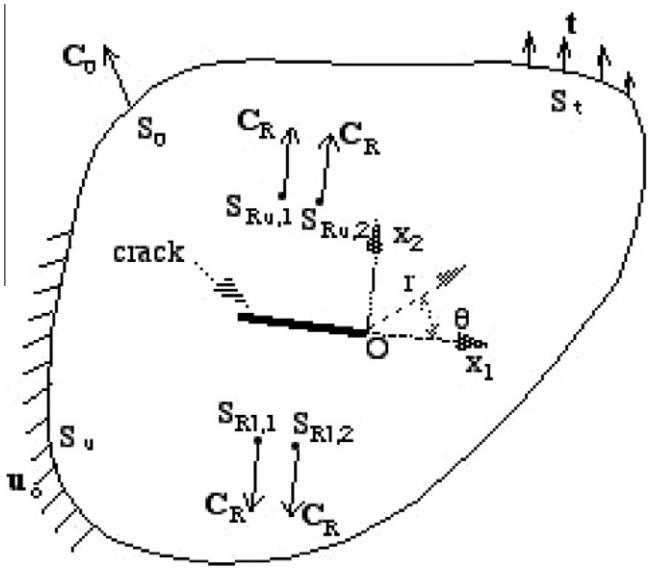

Fig. 4. The crack surface pressures are replaced by $\mathbf{C}_R$ at interior points $S_{Ru,1}$, $S_{Ru,2}$, $S_{Rl,1}$, and $S_{Rl,2}$.

2. Asymptotic near-tip stresses

Consider a crack in a 2-D homogeneous elastic body (Fig. 1). We introduce a local coordinate system originating at the crack tip O, with the crack line lying along the negative x_1-axis. The body is subjected to a system of loads and reaches a deformed state. We assume that the loadings are by surface tractions **t** on a portion of boundary S_t and concentrated force $\mathbf{C}_Q$ at point S_Q, by imposed displacements $\mathbf{u}_o$ on another portion of boundary S_u and, particularly, by nonuniform pressure $p_c(x_1)$ on the crack surfaces S_c.

2.1. Traction-free crack surfaces

For the special condition when the crack surfaces are traction-free, i.e., $p_c(x_1) = 0$, the asymptotic mixed-mode stress field in the immediate neighborhood of the crack tip can be expressed (Williams, 1957) as

$$\sigma_{ij}(r,\theta) = \frac{1}{(2\pi r)^{1/2}}\left[K_I f_{I,ij}(\theta) + K_{II} f_{II,ij}(\theta)\right] + T\delta_{i1}\delta_{j1} + O_{ij}(r^{1/2}) \qquad (1)$$

where σ_{ij} are the Cartesian components of the stress tensor, (r,θ) denote the polar components of the local coordinate, K_I and K_{II} are the SIFs associated with modes I and II respectively, T is the T-stress, δ_{ij} is the Kronecker delta, and $O_{ij}(r^{1/2})$ indicates the higher order term of $r^{1/2}$. Also, the dimensionless angular coefficients $f_{I,ij}(\theta)$ and $f_{II,ij}(\theta)$ are universal functions of θ.

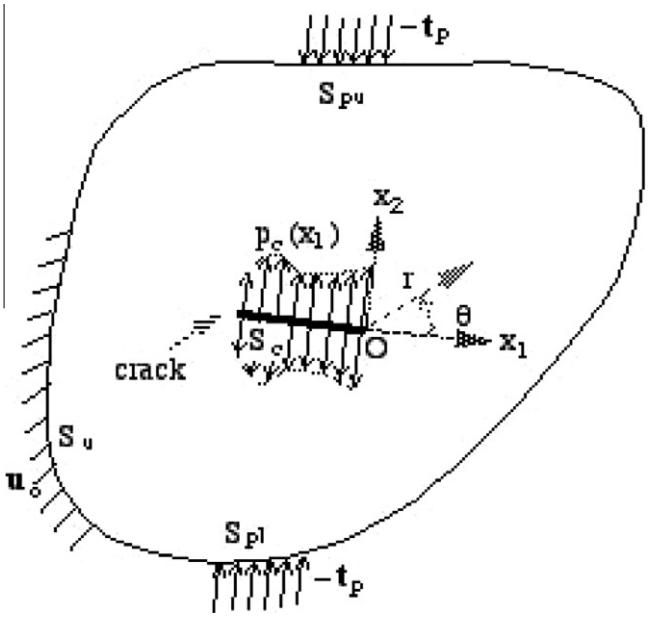

Fig. 5. In this de-singularized loading system, the crack surfaces S_c are subjected to the $p_c(x_1)$, along with the pair of boundary tractions $-\mathbf{t}_p$.

As shown in Eq. (1), there is only one constant term T in the asymptotic stress field. The T-stress contributes uniformly to the stress component σ_{11}, which acts parallel to the plane of the crack. It is also indicated by Eq. (1) that the near-tip stress field is dominated by the leading term $r^{-1/2}$, which accounts for the singular part of the stresses. As a consequence, the contribution of T, which leads the non-singular part of the asymptotic stress field, is relatively small in comparison with the singular part and tends to be neglected numerically.

2.2. Pressurized crack

For problems under the action of prescribed pressures on the crack surfaces, the asymptotic near-tip stress field becomes

$$\sigma_{ij}(r,\theta) = \frac{1}{(2\pi r)^{1/2}}\left[K_I f_{I,ij}(\theta) + K_{II} f_{II,ij}(\theta)\right] + \sigma_{ij} p(r,\theta) \tag{2}$$

where the finite-valued $\sigma^p(r,\theta)$ represents the asymptotic non-singular part of stresses due to the action of all the prescribed loads including $\mathbf{t}$, $\mathbf{C}_Q$, and $p_c(x_1)$. Mathematically, in order to establish the above expression, we need to consider the boundary value problem (BVP) formulated in terms of the Airy stress function with, particularly, the prescribed pressure boundary conditions $p_c(x_1)$. This leads to a solution for K_I, K_{II}, and σ^p consisting of two parts, which

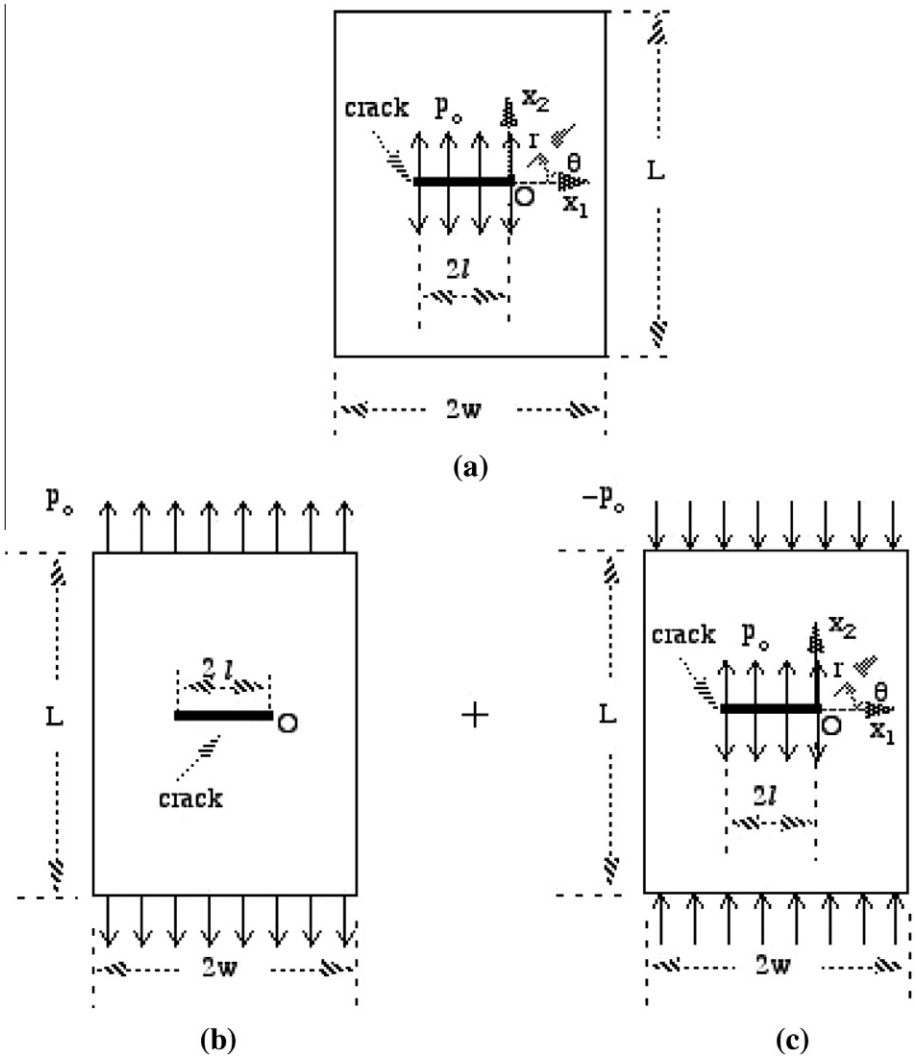

Fig. 6. (a) A central crack subjected to constant crack surface pressure p_o. (b) The Mode I stress field under a far-field uniform tensile load p_o. (c) The specimen is subjected to the de-singularized loading system (Problem 1.1).

are the particular solution associated with $p_c(x_1)$ and the homogeneous solution associated with the traction-free boundary condition. As a result, $\sigma^p(r,\theta)$ represents the convergent series of higher order terms of functions of r and θ in Williams' expansion (starting from the constant terms) and needs to be determined by solving the corresponding BVP. In particular, the T-stress in such a case is defined as (Sham, 1991)

$$T \equiv \sigma_{11} p(r,\theta)|_{r=0} + p_c(x_1)|_{x_1=0} \tag{3}$$

For the special condition when the crack surfaces are traction-free, $\sigma_{ij}^p(r,\theta)$ reduces to $T\delta_{i1\delta j1}$ (i.e., the constant T-stress), as previously described. For the other special condition when the crack tip is locally unloaded (i.e., $p_c(0) = 0$), $T = \sigma_{11}^p(0,\theta)$. For another special condition when the crack is embedded in an infinite medium and subjected only to uniformly distributed pressures along the crack surfaces (i.e., with $p_c(x_1) = p_o$), $\sigma_{ij}^p(r,\theta)$ then appears to be equal to $-p_{o\delta ij}$ (as shown in the Appendix) and, consequently, $T = 0$. This indicates that, in such a uniformly pressurized case, the non-singular stress field is dominated by the constant term $-p_o$. This constant term contributes uniformly to both the stress components σ_{11} and σ_{22}, which act parallel and perpendicular to the plane of the crack respectively.

Note that, as shown in Eqs. (1)/(2), the near-tip stress field is dominated by the leading term $r^{-1/2}$, which corresponds to the singular part of the stresses and can be accurately computed once the SIFs being properly determined with any of the well-developed approaches. As to the non-singular stresses, their contributions in the asymptotic stress field are negligibly small in comparison with the singular part. Therefore, when T/σ_{ij}^p are to be determined numerically by directly subtracting the singular stress components from the near-tip finite element solutions of left hand side quantity $\sigma_{ij}(r,\theta)$ in Eqs. (1)/(2), their results may be relatively inaccurate due to the inevitable truncation error and discretized inaccuracy in finite element calculations.

3. Auxiliary stress field

To avoid the inevitable inaccuracy in evaluation of the near-tip non-singular stresses, we can have the singular part of stresses circumvented by introducing the following concept of auxiliary stress fields. To this end, we take the original boundary value problem in Fig. 1 and replace the crack surface pressures by, say, a pair of tractions $\mathbf{t}_p$ on the portions of boundary S_{pu} and S_{pl}, which are positioned on the upper and lower sides of the crack respectively, as shown in Fig. 2. The magnitude of $\mathbf{t}_p$ is properly specified so that the resulting SIFs associated with tip O are of the same values as those of the original BVP. The corresponding near-tip stress field of this new problem in Fig. 2 is then defined as the auxiliary stress field $\sigma^{(a)}$ and written as

$$\sigma_{ij}^{(a)}(r,\theta) = \frac{1}{(2\pi r)^{1/2}}[K_I f_{I,ij}(\theta) + K_{II} f_{II,ij}(\theta)] + T^{(a)}\delta_{i1}\delta_{j1} + O_{ij}^{(a)}(r^{1/2}) \tag{4}$$

where $T^{(a)}$ is the T-stress and $O_{ij}^{(a)}(r^{1/2})$ is the higher order term of $r^{1/2}$, both corresponding to the auxiliary stress field.

In order to construct the auxiliary stress field, we need to evaluate the corresponding SIFs at the crack tip. This can be done by using a variety of well-developed path-independent contour integrals (e.g., Stern et al., 1976; Chang and Wu, 2007, etc.).

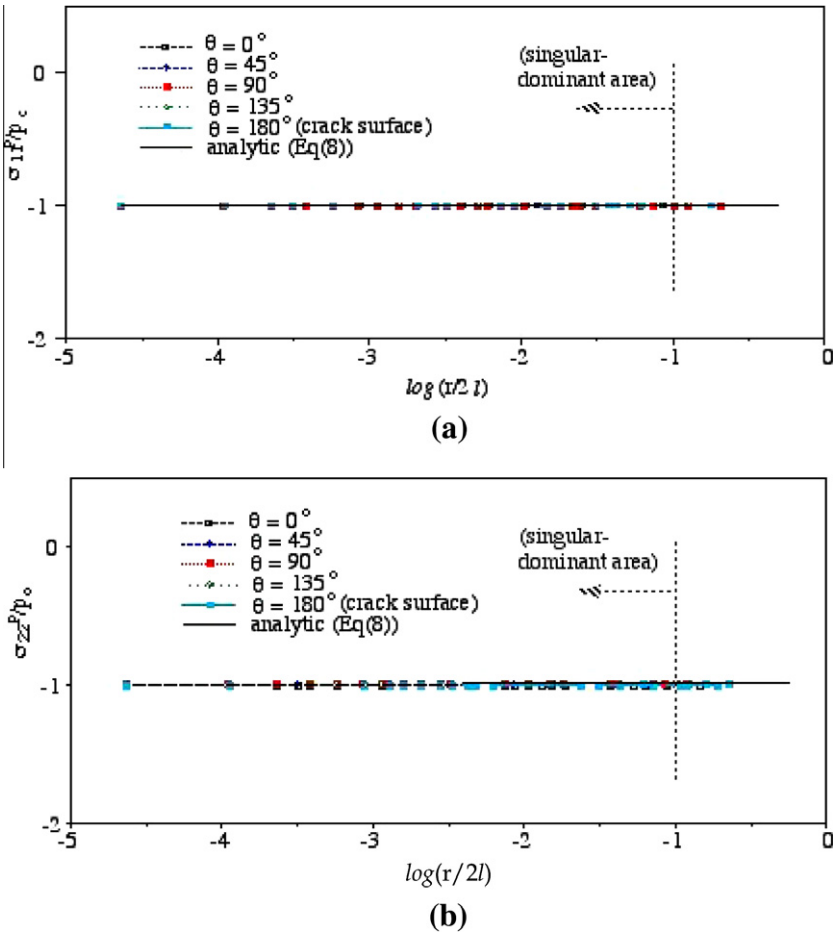

Fig. 7. (a) Radial distributions of near-tip σ_{11}^p/p_o. (b) Radial distributions of near-tip σ_{22}^p/p_o (l/w = 1/10, Problem 1.1).

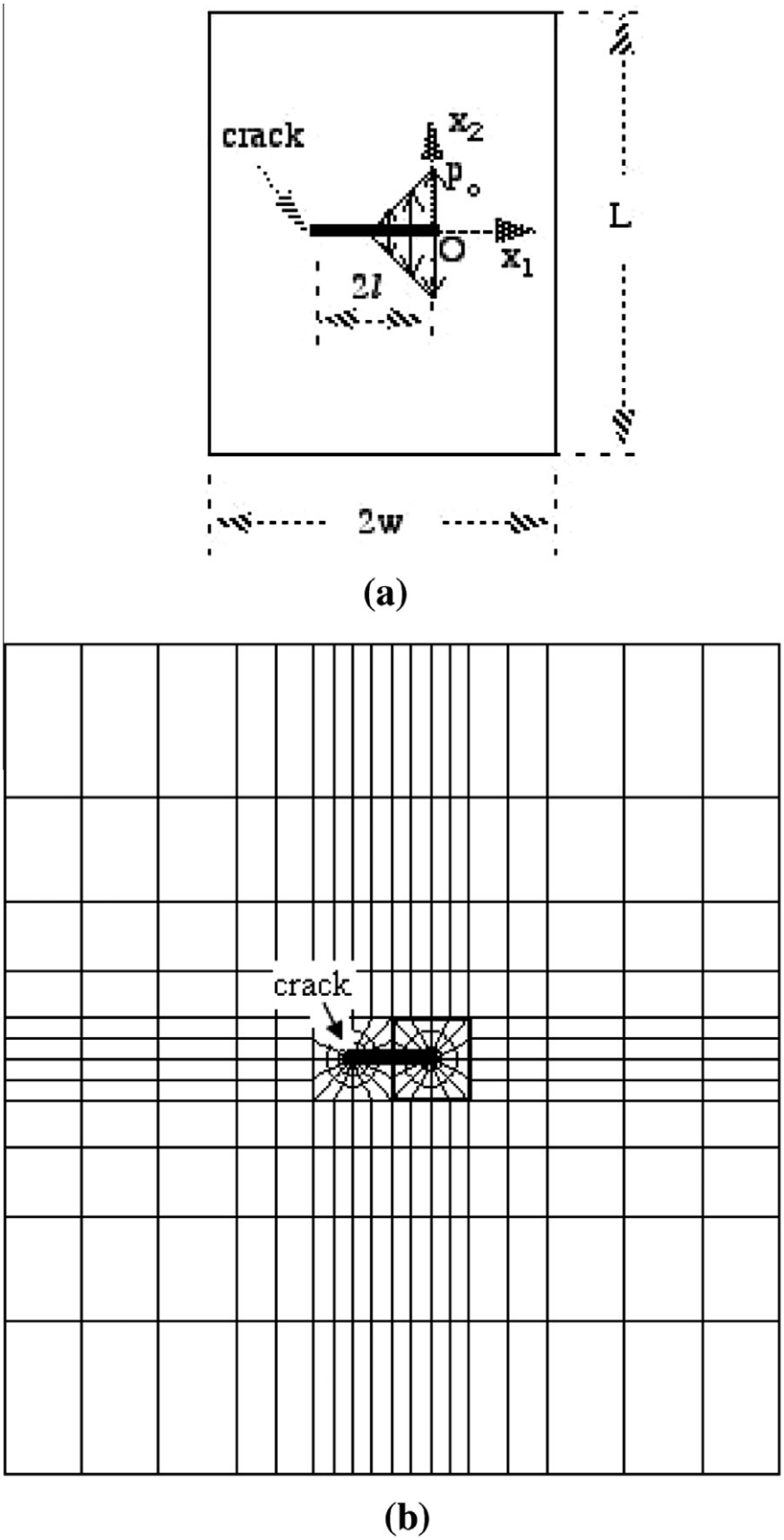

Fig. 8. (a) A central crack subjected to linearly distributed pressure along its right half crack surfaces (Problem 1.2). (b) A typical finite element representation used for the specimen.

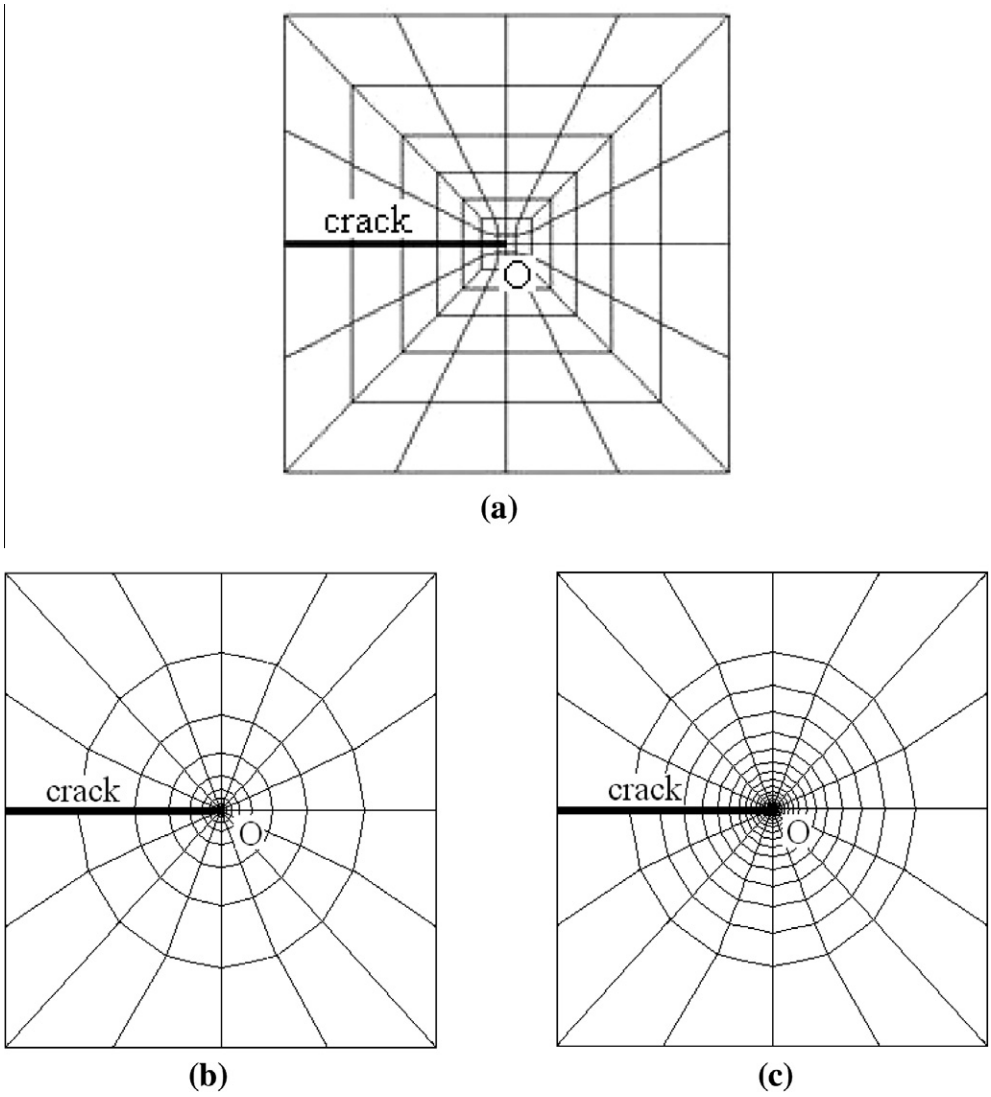

Fig. 9. Three finite element models in the near-tip region for the specimen in Fig 8(a).

It is also noted that the auxiliary stress field can be constructed differently, as long as the corresponding SIFs at tip O are of the same values as those of the original BVP. For one example, instead of the boundary surface tractions $\mathbf{t}_p$ in Fig. 2, we can have the crack surface pressures replaced by a pair of concentrated forces $\mathbf{C}_V$ acting at boundary points S_{Vu} and S_{Vl} (Fig. 3). Further, for another example, the crack surface pressures can be replaced by a set of concentrated forces $\mathbf{C}_R$ applied at four interior points $S_{Ru,1}$, $S_{Ru,2}$, $S_{Rl,1}$, and $S_{Rl,2}$ (Fig. 4). In this sense, there can actually be numerous different selections of auxiliary stress fields. We can therefore take any of them, say, the i-th auxiliary stress field $\sigma^{(ai)}$, and represented it as

$$\sigma_{ij}^{(ai)}(r,\theta) = \frac{1}{(2\pi r)^{1/2}}\left[K_I f_{I,ij}(\theta) + K_{II} f_{II,ij}(\theta)\right] + T^{(ai)}\delta_{i1}\delta_{j1} + O_{ij}^{(ai)}(r^{1/2}) \tag{5}$$

where $T^{(ai)}$ and $O_{ij}^{(ai)}(r^{1/2})$ are the T-stress and the higher order term of $r^{1/2}$ corresponding to $\sigma^{(ai)}$.

4. De-singularized loading system

By taking the ith auxiliary stress field $\sigma^{(ai)}$, and combining Eqs. (2) and (5), we can have the asymptotic non-singular stresses σ^p represented as

$$\sigma_{ij}p(r,\theta) = \sigma_{ij}(r,\theta) - \sigma_{ij}^{(ai)}(r,\theta) + T^{(ai)}\delta_{i1}\delta_{j1} + O_{ij}^{(ai)}(r^{1/2}) \tag{6}$$

Eq. (6) indicates that, once the original and the auxiliary stress fields (i.e., σ and $\sigma^{(ai)}$) are properly determined, the non-singular stresses σ^p can then be calculated. Nevertheless, due to the presence of the near-tip singularity, it is rather difficult to have σ and $\sigma^{(ai)}$ accurately evaluated. Therefore, instead of having σ and $\sigma^{(ai)}$ calculated explicitly, an alternative approach by establishing a 'de-singularized loading system' is proposed as follows.

To this end, we take the difference of the original and the i-th auxiliary stress fields, denoted as σ^{di}, and represent it as

$$\sigma_{ij}^{di}(r,\theta) \equiv \sigma_{ij}(r,\theta) - \sigma_{ij}^{(ai)}(r,\theta) \tag{7}$$

For illustration, we consider the original BVP in Fig. 1 and take the auxiliary stress field in Fig. 2 as an example. It is observed that, by superposition theory, σ^{di} appears to be equivalent to the stress field resulting from the loading system due to the combined action of the crack surface pressure $p_c(x_1)$ and the pair of boundary tractions $-\mathbf{t}_p$ (Fig. 5), which is constructed by taking the difference of the two loading systems in Figs. 1 and 2. Since both the original and auxiliary stress fields possess the same values of SIFs, the singular part of σ^{di} at tip O are thus eliminated. It is therefore anticipated that, under the application of such a de-singularized loading

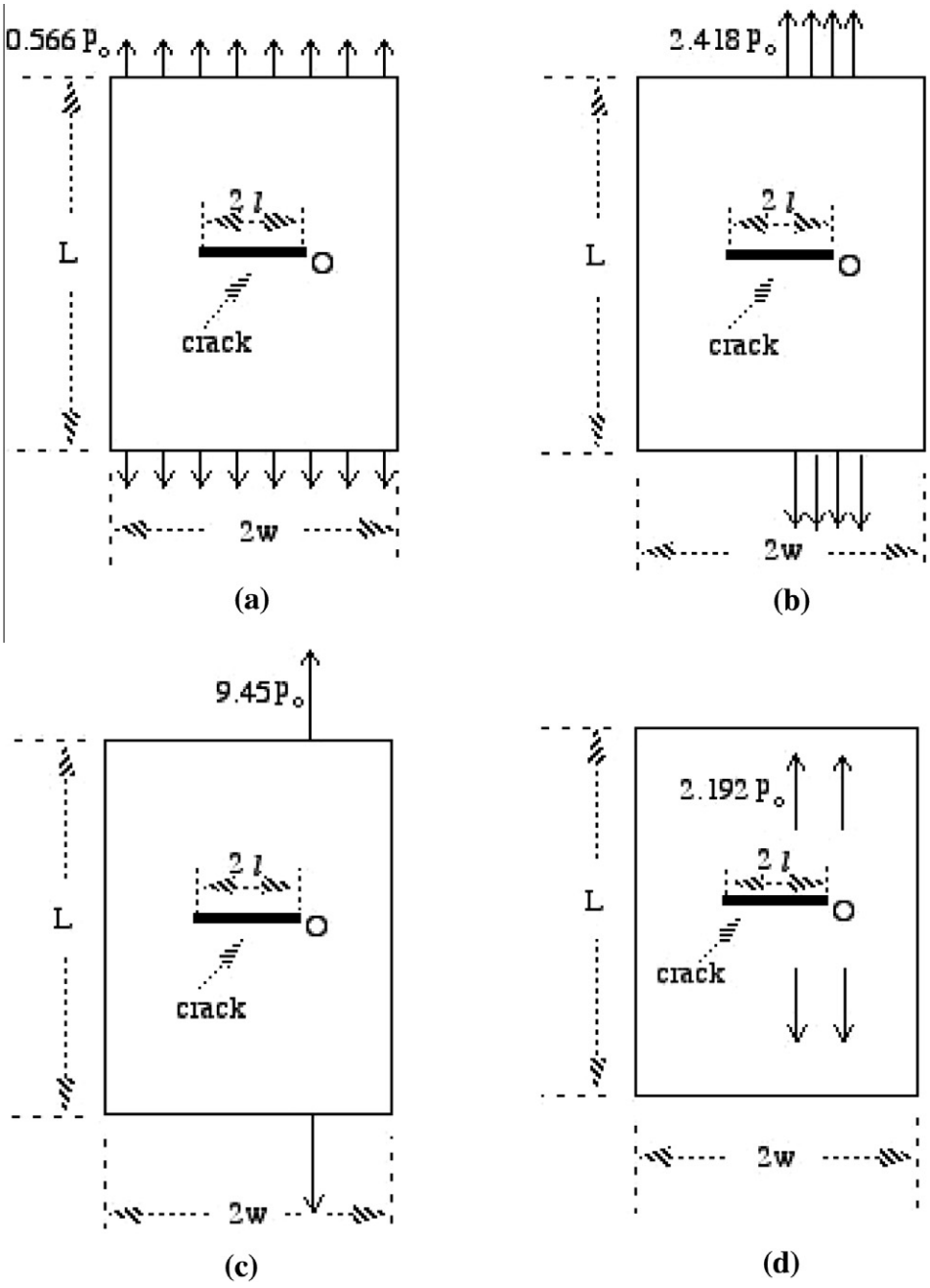

Fig. 10. Four auxiliary stress fields for Problem 1.2.

system in Fig. 5, no singular behavior is involved in σ^{di} at tip O. This de-singular feature implies that σ^{di} can be accurately evaluated by direct use of regular finite element solutions, even in the elements directly adjacent to crack tip O.

Substituting Eq. (7) into Eq. (6) results in

$$\sigma_{ij}^{p}(r,\theta) = \sigma_{ij}^{di}(r,\theta) + T^{(ai)}\delta_{i1}\delta_{j1} + O_{ij}^{(ai)}(r^{1/2}) \tag{8}$$

As indicated by Eq. (8), in addition to σ^{di}, we need to evaluate the T-stress corresponding to the auxiliary stress field in order to determine σ^{p}. This can be done by using a well-developed interaction contour integrals reported in the literature (e.g., Nakamura and Parks, 1991; Sladek et al., 1997; Moon and Earmme, 1998, etc.). In the present investigation the integral provided by ABAQUS version 6.7 has been employed for computation of T-stress. Since the integration is path-independent, accurate values of T can always be obtained without use of singular elements when the first layer of elements adjacent to the crack tip are not selected in the integration contour.

It is also noted that, in addition to σ^{di} and $T^{(ai)}$, an undetermined higher order term associated with the auxiliary stress field $O_{ij}^{(ai)}(r^{1/2})$ is also included in Eq. (8). It is therefore necessary to investigate the effect of this higher order term. This can be done by taking different selections of auxiliary stress fields and cautiously examining the corresponding numerical solutions. As a matter of fact, it is observed that $O_{ij}^{(a)}(r^{1/2})$ makes rather insignificant contributions to the calculation of σ^{p} in the near-tip area. Details of this numerical examination will be illustrated in the following numerical examples.

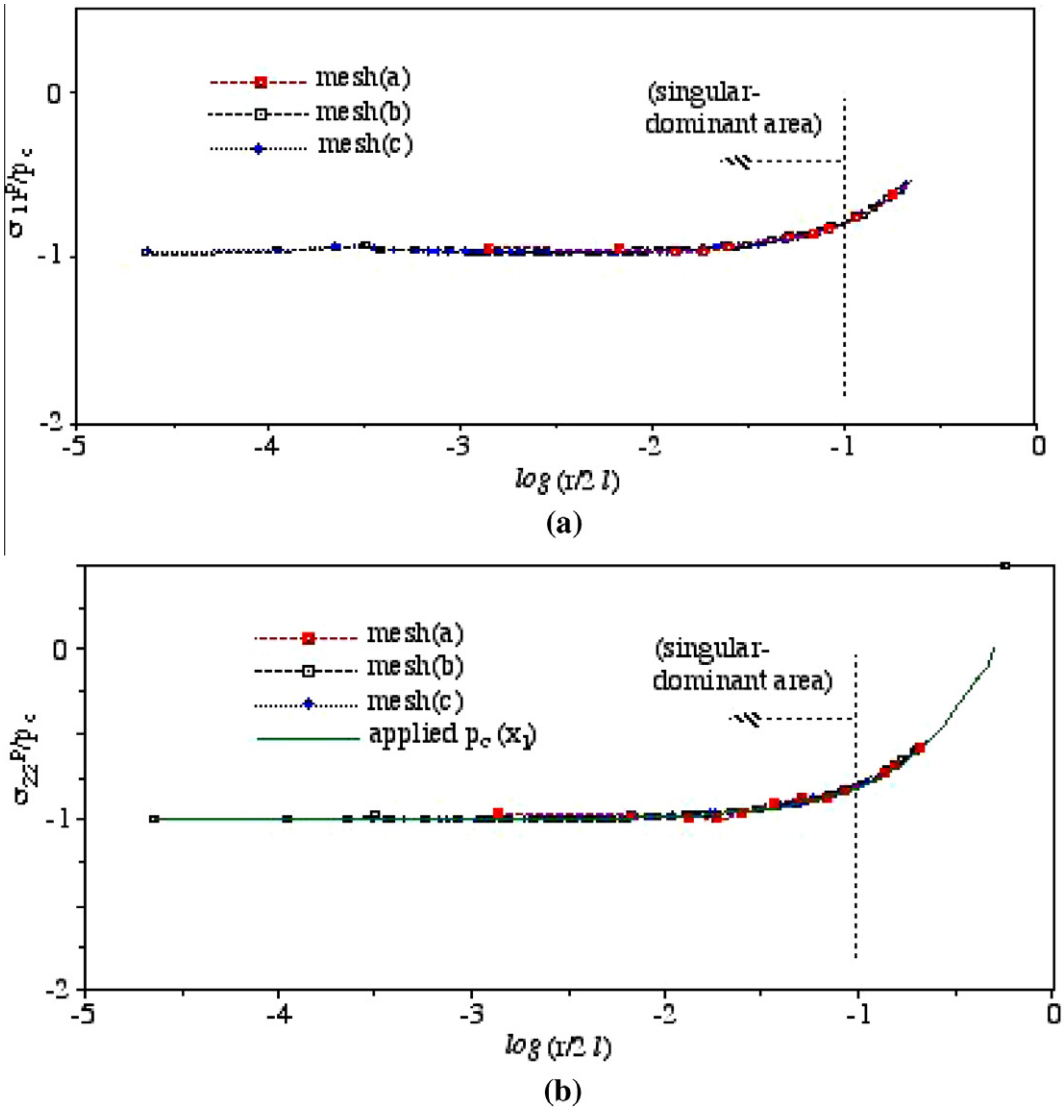

Fig. 11. Radial distributions along the upper crack surface from different FE meshes: (a) near-tip σ_{11}^{P}/p_o, (b) near-tip σ_{22}^{P}/p_o (l/w = 1/10, Problem 1.2).

Table 1
The locations of the loadings (auxiliary stresses, Problem 1.2).

	Loading type	Locations
Fig 10(a)	Distributed tractions	Upper and lower boundaries from (−0.183W,-L/2) to (0.067W,−L/2), from (−0.183W, L/2) to (0.067W, L/2)
Fig 10(b)	Distributed tractions	
Fig 10(c)	Concentrated forces	(0.1W,−L/2), (0.1W,L/2)
Fig 10(d)	Concentrated forces	(-0.05W,-0.213L), (0.067W, −0.213L), (−0.05W,0.213L), (0.067W, 0.213L)

5. Numerical examples

Two sets of numerical example problems are presented in the following two subsections. In the first subsection, a specimen subjected only to crack surface pressures is considered. In the second subsection, specimens subjected to both external loads and crack surface pressures are considered. The problems are analyzed using finite elements. Quadratic elements are used for displacement interpolation in the calculation. No particular singular element is used throughout the study.

5.1. Crack surface pressures

5.1.1. Problem 1.1—constant pressure

This problem is presented to demonstrate the validity of our numerical scheme and verify the accuracy of the calculation. We consider a plane stress specimen with a central crack of length 2l subjected to constant crack surface pressure p_o, as shown in Fig. 6(a). The specimen is modeled with E = 10 MPa and ν = 0.25. When the values of both l/w and l/L are small, analytic solutions for the near-tip non-singular stresses can be written (Appendix) as

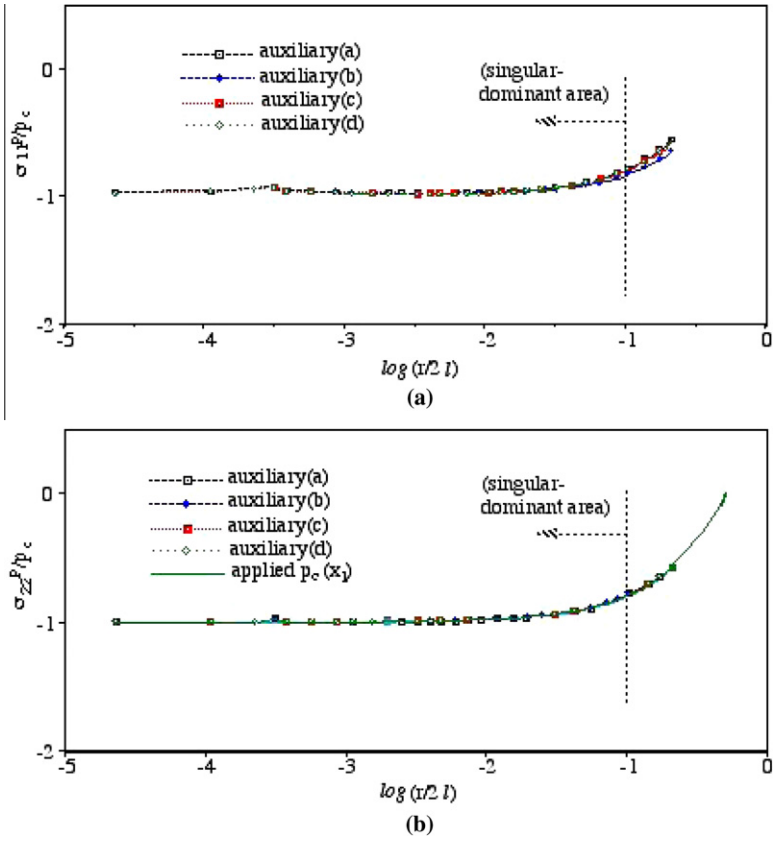

Fig. 12. Radial distributions along the upper crack surface by using different auxiliary solutions: (a) near-tip $\sigma_{11}{}^{P}/p_o$, (b) near-tip $\sigma_{22}{}^{P}/p_o$ (l/w = 1/10, Problem 1.2).

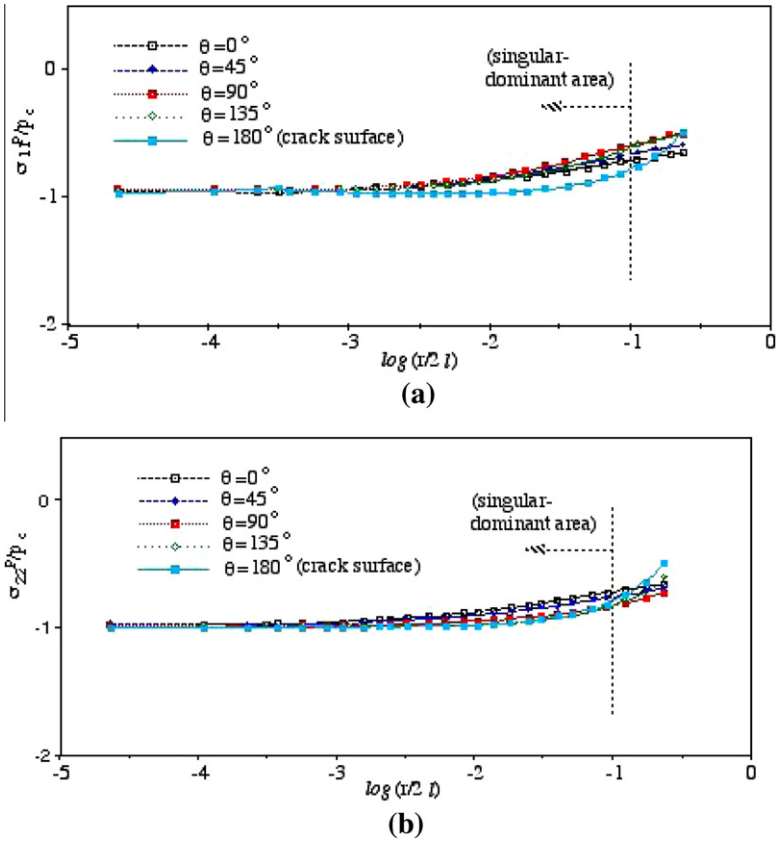

Fig. 13. (a) Radial distributions of near-tip $\sigma_{11}{}^{P}/p_o$, (b) radial distributions of near-tip $\sigma_{22}{}^{P}/p_o$ (l/w = 1/10, Problem 1.2).

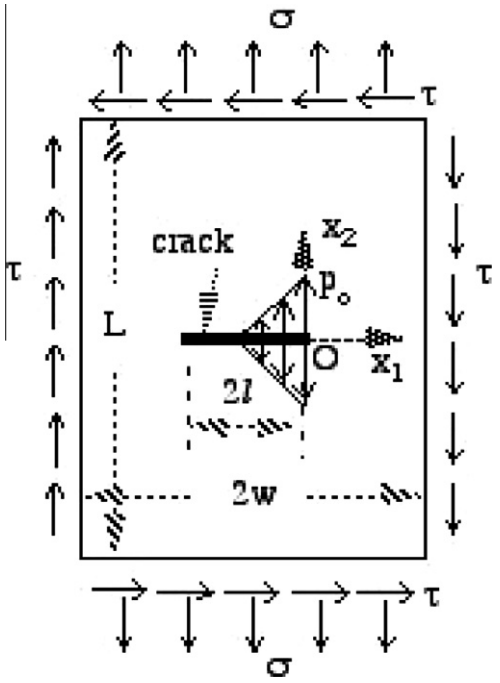

Fig. 14. A centrally cracked specimen subjected to linearly distributed crack surface pressure and external loads (σ, τ) (Problem 2.1).

$$\sigma_{ij}^{p}(r,\theta) = -p_o\sigma_{ij} \tag{9}$$

In the following calculation, an auxiliary stress field is constructed by applying uniform tension p_o along the upper and lower boundaries (Fig. 6(b)). This leads to a de-singularized loading system shown in Fig. 6(c). By solving the problem under this de-singularized loading system using finite elements and then substituting the solutions into Eq. (8), the near-tip non-singular stresses can thus be determined. The results of σ^p versus the scaled local radial distance r/2l are shown in Fig. 7(a) and (b). In the figures, radial distributions of the normalized stress components $\sigma_{11}{}^p/p_o$ and $\sigma_{22}{}^p/p_o$ sampled at the integration points of each element are depicted with respect to various circumferential angles θ. More details about the computation procedure for σ^p will be illustrated in the next example problem. Also shown in the figures are the analytic solutions shown in Eq. (9). The FE results under different angles appear to be almost indistinguishable and all very closed to the analytical solutions. This indicates that the asymptotic behavior of σ^p is accurately simulated in the singular-dominant area (which is in the range within 10% of the crack length, as suggested by Chang and Wu (2007)), even at those points located in the elements directly adjacent to the crack tip.

5.1.2. Problem 1.2—linearly-distributed pressure

In this example, we consider a plane stress specimen with a central crack of length 2l subjected to linearly distributed pressure applied along the right half part of the crack surfaces, with the magnitude at tip O equal to p_o, as shown in Fig. 8(a). Still, The specimen is modeled with E = 10 MPa and ν = 0.25. Also, the specimen

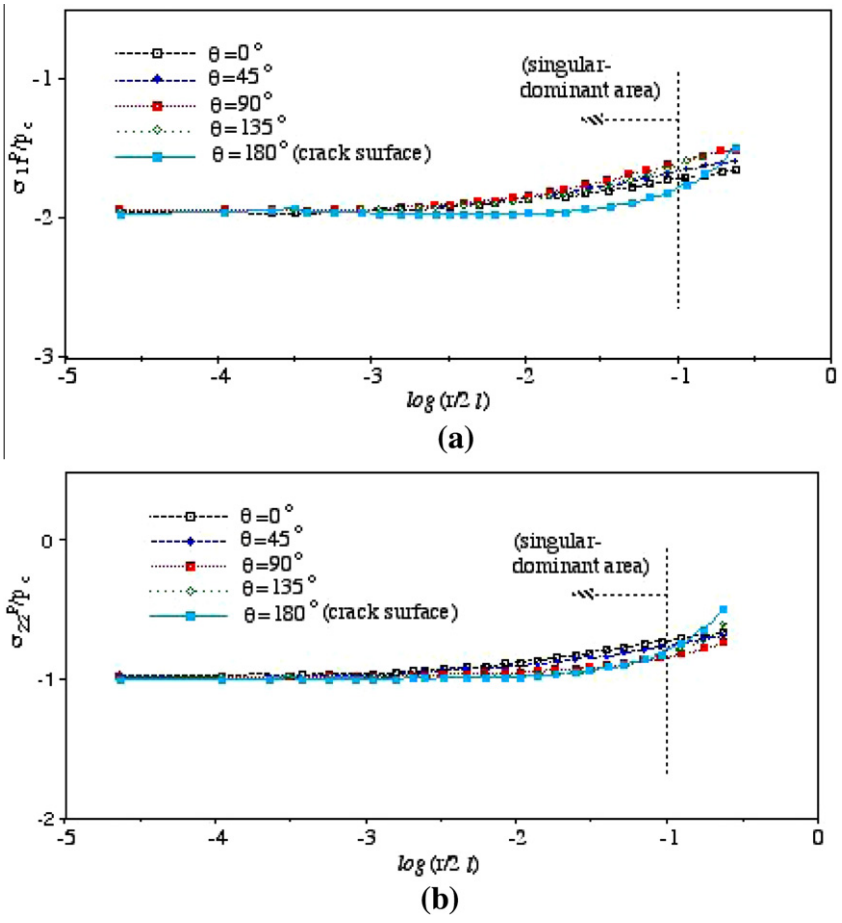

Fig. 15. (a) Radial distributions of near-tip $\sigma_{11}{}^p/p_o$, (b) radial distributions of near-tip $\sigma_{22}{}^p/p_o$ (l/w = 1/10, (σ, τ) = (1,2)p_o, Problem 2.1).

is analyzed by using a typical finite element representation shown in Fig. 8(b). More discussions on the discretized model in the near-tip region will be presented later. Note that both the auxiliary and de-singularized configurations can be analyzed by using the same discretized finite element model, with two different loading conditions. In view of this, the discretization process needs to be carried out for only once in each problem.

The study in this problem is organized as follows. First, the effect of the local near-tip finite element approximation is investigated. Subsequently, the influence due to different selections of auxiliary stress field is examined. Finally, the spatial variation of the resulting σ^p is observed.

To investigate the effect of local mesh refinement around the near-tip area, three finite element models (each with totally 296, 472, and 764 elements, respectively) are defined. Details of the meshes in the vicinity of the crack tip are shown in Fig. 9(a)–(c). The first discretized model mesh(a) is rather coarse and with very different near-tip local element structure from the other two meshes. On the other hand, mesh(b) and the finer mesh(c) are both progressively refined with 12 and 36 layers of elements respectively within the scaled radial range $r/2l = 0.333$. By choosing an auxiliary stress field as shown in, say, Fig. 10(a), the near-tip non-singular stresses σ^p evaluated from the three FE meshes are shown in Fig. 11(a) and (b), where radial distributions of $\sigma_{11}{}^p/p_o$ and $\sigma_{22}{}^p/p_o$ along the upper crack surface (i.e., $\theta = \pi$) are illustrated respectively. The results appear to be very insensitive to the local finite element mesh even in the element directly adjacent to the crack tip. The property of mesh insensitivity for the calculation is thus verified. Also plotted in Fig. 11(b) for comparison is the applied pressure along the upper crack surface. The results show that the FE results of $\sigma_{22}{}^p$ are well consistent with the imposed $p_c(x_1)$ and so the asymptotic behavior is well simulated by the proposed scheme. It is interesting to note that, although $\sigma_{11}{}^p$ and $\sigma_{22}{}^p$ in Fig. 11 both look like remaining almost constant versus $\log(r/2l)$

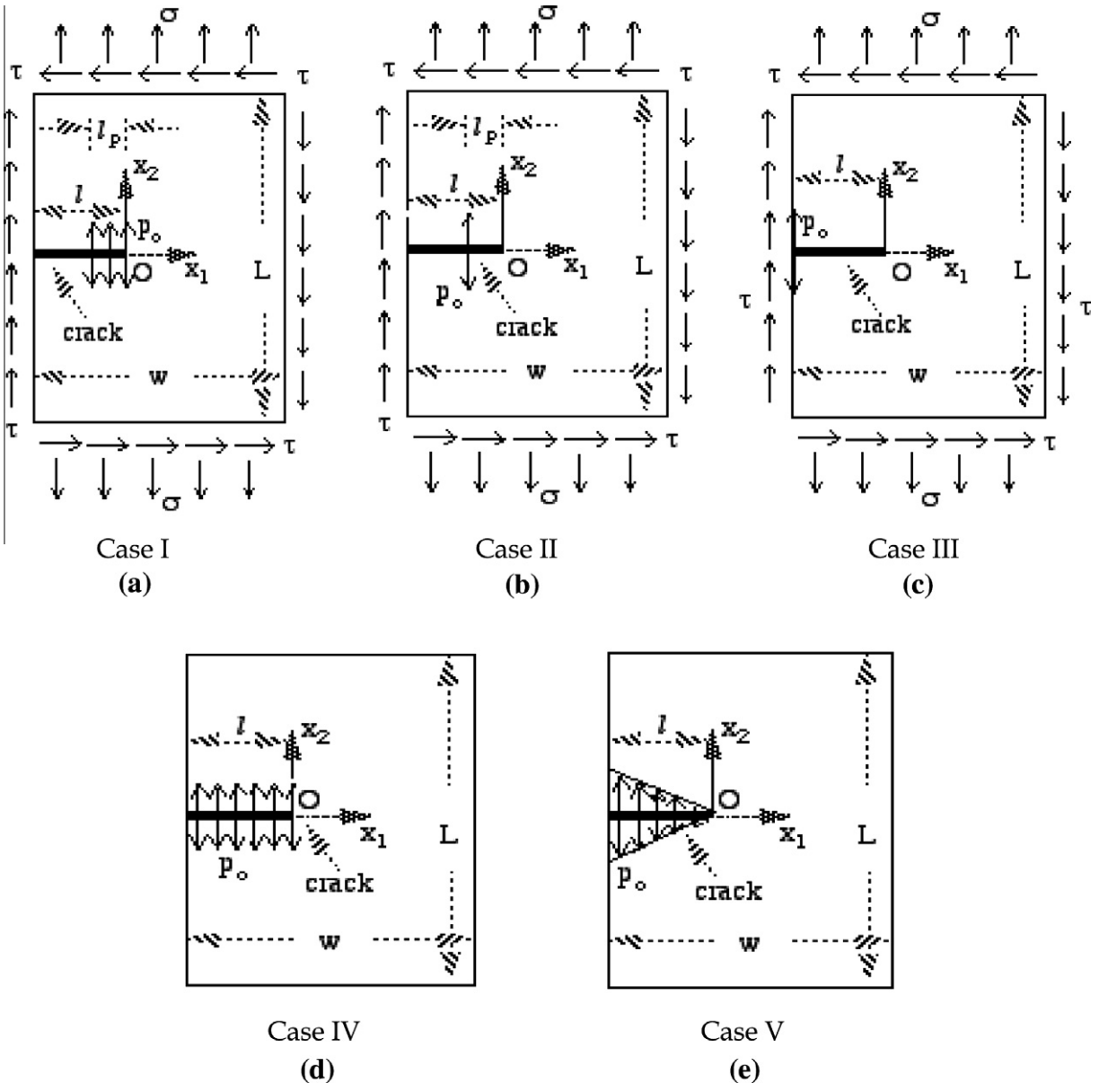

Fig. 16. A single edge notched specimen with a crack of length l subjected to a far-field mixed-mode loading system (σ, τ) (Problem 2.2): (a) uniform crack surface pressure p_o partially loaded in the range of length l_p, (b) a pair of concentrated loads p_o located at a distance l_p away from the tip O, (c) a pair of concentrated loads p_o located at the corner edge of the crack, (d) constant crack surface pressure p_o on the crack surface, $(\sigma, \tau) = (0,0)$, (e) linearly distributed crack surface pressure, $(\sigma, \tau) = (0,0)$.

up to r/2l = 0.01, they actually appear to vary linearly with r/2l. Such linear feature can be illustrated by comparing with the imposed $p_c(x_1)$ shown in Fig. 8(a).

To examine the influence due to different selections of auxiliary stress fields, four auxiliary stresses as shown in Fig. 10(a)–(d) are defined for the calculation. These auxiliary stresses are constructed by imposing either distributed tractions or concentrated forces, which can be located either along the boundary or inside the body. The locations of these loadings are listed in Table 1. Note that the magnitude of the loads for these auxiliary stresses can be easily determined since they are directly proportional to the SIFs. The near-tip non-singular stresses are then evaluated by using these four auxiliary stresses and the results along the upper crack surface are shown in Fig. 12(a) and (b). It is observed that all the auxiliary stresses yield almost indistinguishable results for both $\sigma_{11}{}^{p}$ and $\sigma_{22}{}^{p}$ in the singular-dominant region. Such independent feature indicates that the undetermined higher order term $O_{ij}^{(ai)}(r^{1/2})$ in Eq. (8) makes rather insignificant contributions to the calculation of σ^p in the singular-dominant region and so can be neglected.

Since the concept of evaluation of σ^p is originally presented in this paper, there is no analytical or numerical solution for this problem with which direct test of the above computation scheme can be carried out. Nevertheless, the numerical results show that the calculations are rather insensitive to the near-tip FE mesh. Also, the computed values from different auxiliary stress fields appear to be well consistent with each other within the singular-dominant region. Further, the imposed crack surface pressures are observed to be well simulated in the calculation. The feasibility of the proposed scheme can thus be appropriately demonstrated by the above observations and comparisons.

As an aside, the radial distributions of σ^p corresponding to different circumferential angles θ are plotted in Fig. 13(a) and (b). It is observed that the absolute magnitudes of both $\sigma_{11}{}^{p}$ and $\sigma_{22}{}^{p}$ are peaked at the crack tip, with their values reach up to p_o and then decrease gradually as the radial distance increases. Such spatially varying behavior of σ^p is actually due to the influence of the higher order terms. Under the action of nonuniform crack surface pressures, some of the non-singular coefficients in William's expansion may be relatively larger than the constant terms so that their influence becomes rather significant even though the radial distance at which the stress components estimated is very small. This appears to be different from the behavior of constant T-stress, contributed only to the component of σ_{11}, for the condition of traction-free cracks.

5.2. External Loads and Crack Surface Pressures

5.2.1. Problem 2.1—central-cracked specimen

We have a plane stress specimen with a central crack of length 2l subjected to linearly distributed pressure, as well as a far-field mixed-mode loading system (σ, τ), as shown in Fig. 14.

Since the specimen is subjected to the same crack surface pressure as that in Problem 1.2, both problems can thus be solved by using the same auxiliary stresses and, consequently, the same de-singularized loading system. Hence, the near-tip non-singular stresses σ^p can then be determined by taking the results of Problem 1.2 and superposing with the T-stress due to the far-field loading system (σ, τ), By comparing the results of the present problem (Fig. 15(a) and (b)) with those of Problem 1.2 (Fig. 13(a) and (b)), it is observed that the values of $\sigma_{11}{}^{p}$ for the two problems are

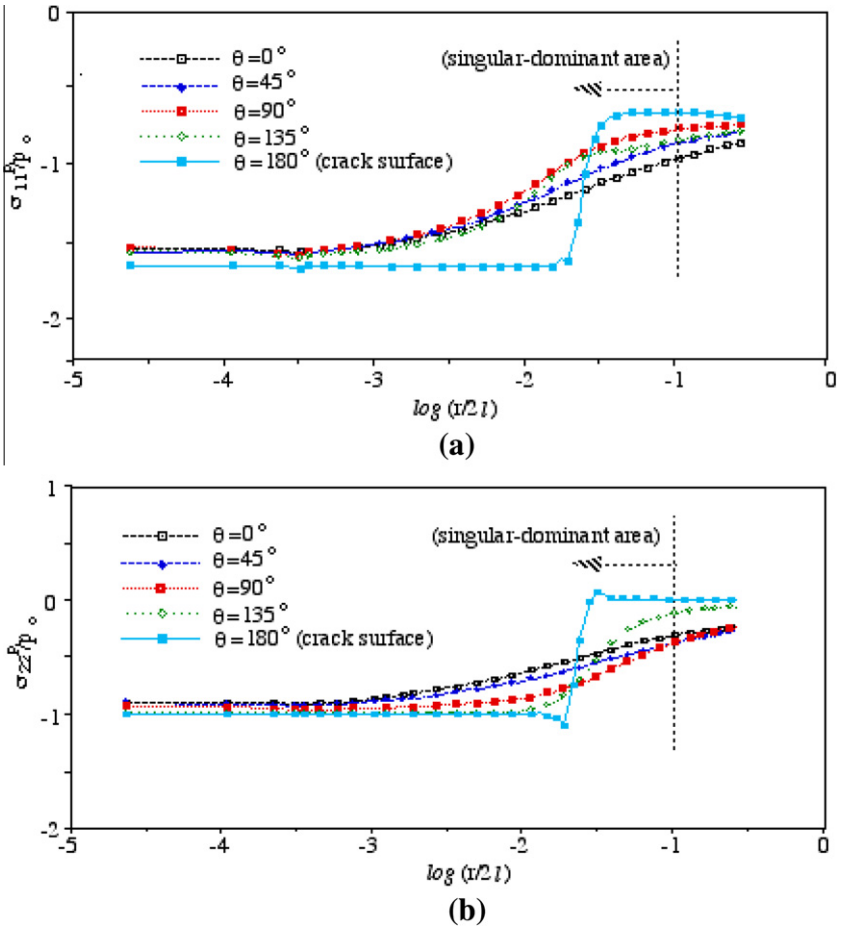

Fig. 17. (a) Radial distributions of near-tip $\sigma_{11}{}^{p}/p_o$, (b) radial distributions of near-tip $\sigma_{22}{}^{p}/p_o$ (l/w = 1/10, $l_p/2l$ = 0.024, (σ, τ) = (1,2)p_o, Case I, Problem 2.2).

different by a constant $-\sigma$, which appears to depend on the far-field load. On the other hand, σ_{22}^{p} remains unchanged as long as the crack surface pressure remains the same.

5.2.2. Problem 2.2—single edge notched specimen

We have a single edge notched specimen with a crack of length l subjected to a far-field mixed-mode loading system (σ, τ). In the following calculations, five instances of crack surface pressures are considered.

In the first instance (Case I), the crack surfaces are subjected to the uniform pressure p_o that is partially loaded within the range of length l_p, as shown in Fig. 16(a). The radial distributions of σ^p corresponding to different circumferential angles θ are calculated with our proposed scheme and shown in Fig. 17(a) and (b). The results show that, along the upper crack surface (i.e., $\theta = 180^o$), both σ_{11}^{p} and σ_{22}^{p} remain constant within the range of length l_p under this partially-loaded constant pressure, then increase abruptly by an amount of p_o and stay (almost) invariant as the radial distance increases. In particular, the FE results of σ_{22}^{p} are well consistent with the imposed $p_c(x_1)$ in the whole range of singular-dominant area, even in the element directly adjacent to the crack tip. It is also observed that, as θ decreases (i.e., away from the crack surface), the stresses appear to distribute more smoothly in the radial direction, as anticipated.

In the second loading instance (Case II), the crack surfaces are subjected to a pair of concentrated loads p_o that is located at a distance l_p away from the crack tip, as shown in Fig. 16(b). A comparison of the FE results for σ^p corresponding to different circumferential angles θ is made and shown in Fig. 18(a) and (b). It is shown in the figures that both σ_{11}^{p} and σ_{22}^{p} remain constant along the upper crack surface (i.e., $\theta = 180^o$), except in the neighborhood of $r = l_p$. where an abrupt increase to a relatively large value (analytically approaching to infinity) is observed due to the presence of the concentrated load. Moreover, the radial distribution of σ^p appears to be more and more smooth as θ decreases. This result indicates that, although the concentrated load leads to singular stresses at $r = l_p$, the non-singular stress field elsewhere can be properly determined with the presented approach.

In the third loading instance (Case III), the crack surfaces are subjected to a pair of concentrated loads p_o located at the corner edge of the crack, as shown in Fig. 16(c). The FE results for σ^p corresponding to different circumferential angles θ are plotted in Fig. 19(a) and (b). It is shown in Fig. 19(a) that the values of σ_{11}^{p} remain almost constant within the range of $r/2l < 0.01$ for all angles. Also, the results of σ_{22}^{p} are observed to be vanishingly small within almost the same range. It is therefore indicated that, when the load is away enough from the crack tip, the feature exhibited by the non-singular stresses appear to be very similar to that of the T-stress. The feasibility of our presented approach is thus further demonstrated in this problem.

The results of σ^p can also be used to calculate the T-stress. In the fourth instance (Case IV), the crack surfaces are subjected to the constant pressure p_o, as shown in Fig. 16(d). As illustrated in Eq. (3), the T-stress can be evaluated by taking the FE result of σ_{11}^{p} at the crack tip (in this instance, r is taken as $10^{-4}\, l$ and considered along the upper crack surface, i.e., $\theta = 180^o$, and then added by $p_c(0) = p_o$. The results of $\sigma_{11}^{p}(10^{-4}l, 180^o) + p_o$ corresponding to different ratios of l/w are tabulated in Table 2. Also listed in the table

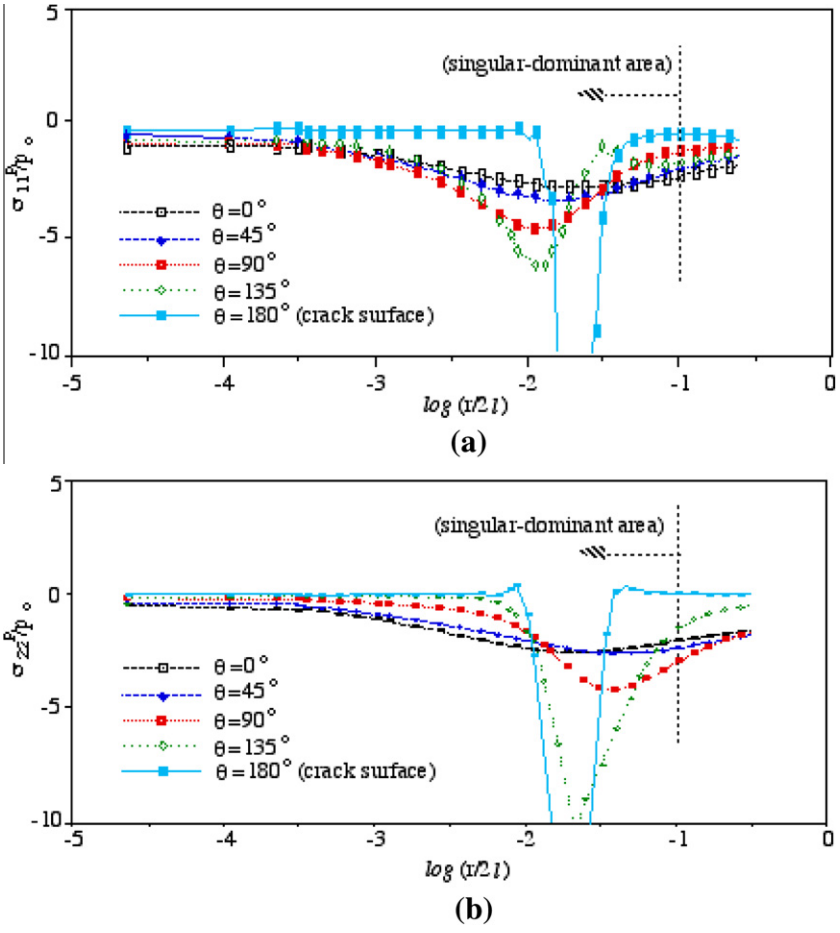

Fig. 18. (a) Radial distributions of near-tip σ_{11}^{p}/p_o, (b) radial distributions of near-tip σ_{22}^{p}/p_o ($l/w = 1/10$, $l_p/2l = 0.024$, $(\sigma, \tau) = (1,2)p_o$, Case II, Problem 2.2).

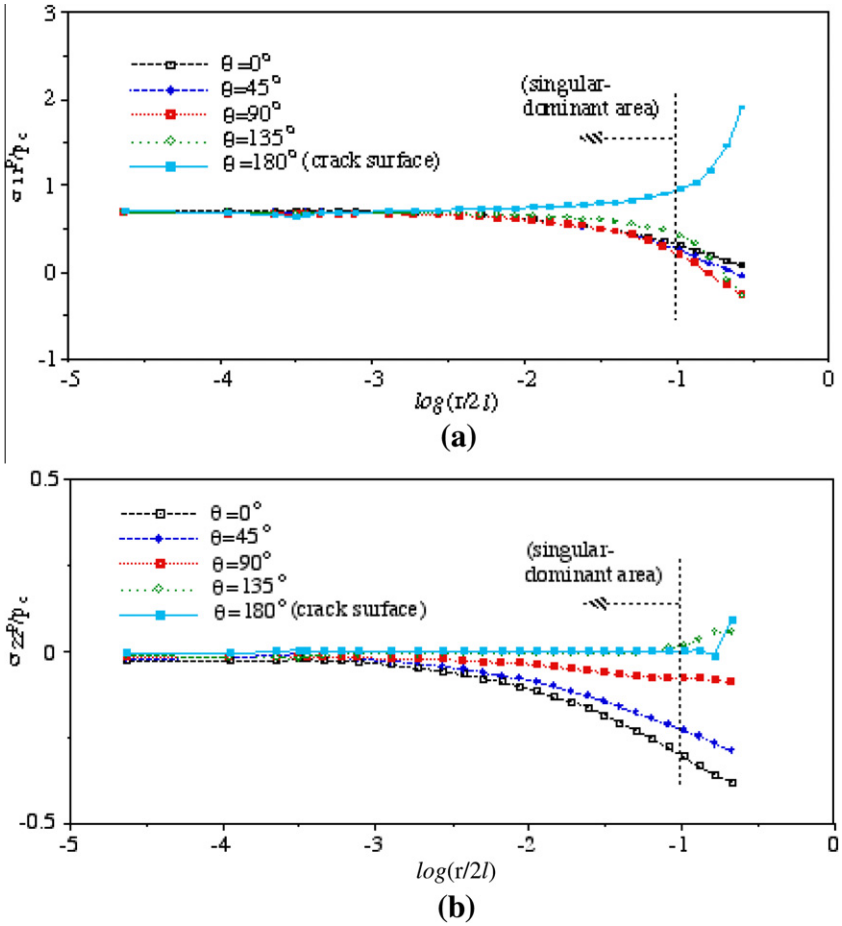

Fig. 19. (a) Radial distributions of near-tip $\sigma_{11}{}^{p}/p_o$, (b) radial distributions of near-tip $\sigma_{22}{}^{p}/p_o$ ($l/w = 1/10$, $(\sigma, \tau) = (0.5,1)p_o$, Case III, Problem 2.2).

are the results of T from Wang (2002), where an interaction integral (Nakamura and Parks, 1991) is used for the calculation. The numerical results from both approaches are observed to be well consistent with each other, with maximum deviation under 3%.

In Case V, linearly distributed crack surface pressure is considered, as shown in Fig. 16(e). Similarly, the T-stress can be evaluated by taking the FE result of $\sigma_{11}{}^{p}$ at the crack tip (still, $r = 10^{-4}\ l$ and $\theta = 180°$, and then added by $p_c(0) = 0$. The results of $\sigma_{11}{}^{p}(10^{-4}l,180°)$ corresponding to different ratios of l/w are tabulated in Table 3. Also listed in the table for comparison are the results of T from Wang (2002). The maximum deviation from both approaches are observed to be under 3%. The feasibility of this proposed approach is thus further demonstrated from the comparison study.

It is well acknowledged that the T-stress has significant effects on various aspects of fracture of engineering components and such effects have been experimentally evident in the literature when the crack surfaces are traction-free. Nevertheless, for nonuniformly pressurized cracks, in addition to T, $p_c(x_1)$ and the higher order terms also contribute to both $\sigma_{11}{}^{p}$ and $\sigma_{11}{}^{p}$, as observed from the above numerical results. It is therefore important to investigate whether the relations between T and the fracture of engineering components are still valid under such conditions. However, we can hardly make any conclusions on this subject from currently available experimental data since most of them were calibrated under the traction-free conditions. Therefore, in order to examine the significance of T and/or σ^{p} on the fracture of engineering components, further information from experiments in this field is obviously required in future study.

Table 2
The T-stress (Case IV, Problem 2.2).

l/w	0.2	0.4	0.6	0.8
$[\sigma_{11}{}^{p}(10^{-4}l,180°) + p_o]/p_o$	0.4078	0.4154	1.0278	6.9754
T/p_o (Wang, 2002)	0.4050	0.4217	1.0405	6.8297

Table 3
The T-stress (Case V, Problem 2.2).

l/w	0.2	0.4	0.6	0.8
$[\sigma_{11}{}^{p}(10^{-4}l,180°)]/p_o$	0.2799	0.2889	0.6981	4.4538
T/p_o (Wang, 2002)	0.2831	0.2953	0.7019	4.5876

6. Conclusion

When the crack surfaces are traction-free, there is only one constant term T that contributes uniformly to the stress σ_{11} in the near-tip stress field. For pressurized cracks, the non-singular parts of the near-tip stresses appear to be more complicated and is no longer characterized only by the constant T. In this work, a numerical approach is developed for calculation of the non-singular parts of the asymptotic near-tip stresses under the action of nonuniform crack surface pressures. By introducing the concept of auxiliary stress fields, a de-singularized loading system can be established. With this de-singularized loading system, the near-tip non-singular stress field for pressurized cracks can then be directly extracted

from regular numerical solutions such as finite elements. The auxiliary stress fields can be easily constructed and this presented scheme is applicable for problems with arbitrary spatial distribution of crack surface pressures. No particular singular elements are required in the calculation.

Acknowledgment

This work has been partially supported by National Science Council Grant No. NSC 100-2221-E-008-071 to National Central University.

Appendix A

We consider a plane stress specimen with a central crack of length $2l$ subjected to constant crack surface pressure p_o, as shown in Fig. 6(a). When the values of both l/w and l/L are small, this corresponds to the condition with a crack embedded in an infinite medium and subjected only to uniformly distributed pressure along the crack surfaces.

The non-singular part of stresses at tip O can be determined by using the concept of superposition theory. With this theory, we can have the stress field due to the action of the crack surface pressure replaced by the sum of those shown in Fig. 6(b) and (c). In Fig. 6(b), the specimen is subjected to the far-field uniform tensile load p_o, which corresponds to a Mode I stress field and the asymptotic stresses near crack tip O can be expressed as (Broek, 1986)

$$\sigma_{ij}(r,\theta) = \left(\frac{l}{2r}\right)^{1/2} p_o f_{I,ij}(\theta) - p_o \delta_{i1}\delta_{j1} + O(r^{1/2}) \tag{A.1}$$

As to the specimen in Fig. 6(c), the crack is inactivated due to the combined action of the far-field $-p_o$ and the crack surface pressure p_o. The specimen is then stressed homogeneously by the compressive load $-p_o$ in the x_2-direction, i.e.,

$$\sigma_{ij}(r,\theta) = -p_o \delta_{i2}\delta_{j2}. \tag{A.2}$$

As a result, by taking the summation of Eqs. (A.1) and (A.2), we then have the asymptotic stresses for the uniformly pressurized crack in Fig. 6(a) be expressed as

$$\sigma_{ij}(r,\theta) = \left(\frac{l}{2r}\right)^{1/2} p_o f_{I,ij}(\theta) - p_o \delta_{ij} + O(r^{1/2}) \tag{A.3}$$

References

Broberg, K.B., 2005. A note on T-stress determination using dislocation arrays. Int. J. Fract. 131, 1–14.
Broek, D., 1986. Elementary Engineering Fracture Mechanics, fourth ed. Martinus Nijhoff Publishers.
Chang, J.H., Wu, D.J., 2007. Computation of mixed-mode stress intensity factors for curved cracks in anisotropic elastic solids. Eng. Fract. Mech. 74, 1360–1372.
Chen, Y.Z., Lin, X.Y., Wang, Z.X., 2010. A rigorous derivation for T-stress in line crack problem. Eng. Fract. Mech. 77, 753–757.
Eischen, J.W., 1987. An improved method for computing the J_2 integral. Eng. Fract. Mech. 26, 691–700.
Fett, T., Rizzi, G., 2005. Weight functions for stress intensity factors and T-stress for oblique cracks in a half-space. Int. J. Fract. 132, L9–L16.
Jogdand, P.V., Murthy, K.S.R.K., 2010. A finite element based interior collocation method for the computation of stress intensity factors and T-stresses. Eng. Fract. Mech. 77, 1116–1127.
Moon, H.J., Earmme, Y.Y., 1998. Calculation of elastic T -stresses near interface crack tip under in-plane and anti-plane loading. Int. J. Fract. 91, 179–195.
Nakamura, T., Parks, D.M., 1991. Determination of elastic T-stress along 3-D crack fronts using an interaction integral. Int. J. Sol. Struct. 29, 1597–1611.
Sham, T.L., 1991. The determination of the elastic T-term using higher order weight functions. Int. J. Fract. 48, 81–102.
Sladek, J., Sladek, V., Fedelinski, P., 1997. Contour integrals for mixed-mode crack analysis: effect of nonsingular terms. Theo. Appl. Fract. Mech. 27, 115–127.
Stern, M., Becker, E.B., Dunham, R.S., 1976. A contour integral computation of mixed-mode stress intensity factors. Int. J. Fract. 12, 359–368.
Wang, X., 2002. Elastic T-stress for cracks in test specimens subjected to non-uniform stress distributions. Eng. Fract. Mech. 69, 1339–1352.
Wang, X., 2003. Elastic T-stress solutions for semi-elliptical surface cracks in finite thickness plates. Eng. Fract. Mech. 70, 731–756.
Wang, Y.Y., Parks, D.M., 1992. Evaluation of the elastic T-stress in surface-cracked plates using the line-spring method. Int. J. Fract. 56, 25–40.
Williams, M.L., 1957. On the stress distribution at the base of a stationary crack. J. Appl. Mech. 24, 109–114.